European Journal of Mechanics / B Fluids 67 (2018) 404–416

Contents lists available at ScienceDirect

European Journal of Mechanics / B Fluids

journal homepage: www.elsevier.com/locate/ejmflu

Use of digitally filtered inflow conditions for LES of flows over backward facing steps

Kalyana Chakravarthy *, Konark Arora, Debasis Chakraborty

Defence Research and Development Laboratory, Kanchanbagh, Hyderabad, India

ARTICLE INFO

Article history:
Received 2 March 2017
Received in revised form 22 September 2017
Accepted 7 October 2017
Available online 2 November 2017

Keywords:
Large eddy simulations
Inflow conditions
Compressible turbulence
Hybrid solver
Separated flows

ABSTRACT

Large eddy simulations (LES) of subsonic and supersonic boundary layers separating at backward facing steps are performed for validating a hybrid flow solver and testing the digital filtering approach for specifying the inflow turbulence. The broadband spectra of eddies in the approaching boundary layers resulting from filtering properly trigger the shear layer instabilities leading to significant improvements in predictions of first and second order turbulence statistics when compared to those resulting from use of uncorrelated noise for generating inflow turbulence. This seems to be true even though the distance between the inflow boundary and the step is about the same or less than in most of the LES of this kind of flows reported in literature and not sufficient to establish an equilibrium boundary layer with correct phase information before the flow reaches the step. The density/entropy disturbances resulting from non-solenoidal inflow do not seem to adversely affect the predictions in the subsonic case. The digital filtering approach does, however, generate acoustic disturbances that contaminate the expansion fan generated at the corner and lead to slight overpredictions in turbulence levels downstream in the supersonic case.

1. Introduction

Inflow conditions are critical for accuracy of large eddy simulations (LES) of spatial evolving flows. Several inflow specification techniques developed over the years continue to be refined as there is no optimal choice as yet.

Lund and coworkers [1] proposed the recycling–rescaling method for turbulence inflow specification based on earlier work of Spalart [2]. Since the scaling laws for equilibrium boundary layers are known, this method and its variants have been preferred for simulating them using LES [3–6]. Ways to specify thermodynamic variables in case of compressible flows with in this approach have also been developed successfully [7–9]. As Ferrante and Elgobashi [10] noted, proper initialization is necessary to ensure fast and sustainable realization of turbulence between the inlet and the recycle planes. Extensions to handle incoming boundary layers with axial pressure gradients, to authors' knowledge, have not been explored yet. These methods may also introduce spurious dynamics at a frequency corresponding to convective time scale of the recycle zone [11–13].

For many practical applications of LES, methods that can broadly be termed as synthetic turbulence approaches are simpler than those based on recycling or precursor simulations. Synthetic turbulence approaches seek to create large scale eddies that would set up the energy cascade and a broadband spectrum. The small scale dynamics have shorter time scales and adjust very quickly. Different ways of generating synthetic turbulence have been developed. The synthetic eddy method [11,14] uses randomly distributed eddies introduced near the inlet whose collective effect conditioned by the prescribed statistics (second order moments of the velocity field) determines the instantaneous inflow conditions. These eddies can be viewed as coherent structures [15] or vortex elements in the classical vortex dynamics description of turbulence. Coherent structures generated at the inlet produce and sustain turbulence with in a short distance from inlet boundary. This approach has been used very effectively for a range of compressible flow problems to generate inflow conditions at interfaces between Reynolds averaged Navier–Stokes (RANS) based approaches and LES in zonal RANS–LES methods [16–19]. Initial work [16,17] relied on the control planes approach of Spille-Kohoff and Kaltenbach [20] where additional forcing on planes parallel to inflow plane is used to counter the initial amplification or decay of synthetic turbulence and achieve target Reynolds stress profiles quickly. Later, a reformulated synthetic turbulence generation (RSTG) method [18] was introduced which avoids the complexity of the control planes approaches. This method help realize equilibrium boundary layers over very short distances and has also been demonstrated for flows with pressure gradients [19].

Purely mathematical methods are generally variants of three original approaches. Gao and Mashayek [21] developed a simple method of generating inflow turbulence with given second

* Corresponding author.
E-mail address: v_kalyana_chakravarthy@yahoo.co.in (K. Chakravarthy).

https://doi.org/10.1016/j.euromechflu.2017.10.006
0997-7546/

Nomenclature

C_f	friction coefficient
C_p	coefficient of pressure
ER	expansion ratio
h	step height
M	Mach number
p	pressure
p'	pressure fluctuation
Re_h	Reynolds number based on step height, free stream conditions
ρ	density
ρ'	RMS value of density
t	time
U_o	inflow velocity outside the boundary layer
X_r	reattachment length
x, y, z	streamwise, wall-normal and spanwise coordinates
U, V, W	mean streamwise, wall-normal and spanwise velocities
u', v', w'	RMS values of streamwise, wall-normal and spanwise fluctuating velocities
$\langle u'v' \rangle$	Reynolds stress
γ	ratio of specific heats

moments and it has been used successfully in a few studies but in this approach, though three different time scales are used for correlating the three velocity components, the correlation is only along the flow direction. The temporal correlation at the inlet translates into a spatial correlation along the flow direction. There is no spatial structure/correlation in any direction perpendicular to the inflow plane. The same is true with the turbulence forcing scheme introduced by Volavy and coworkers [22]. Despite this fact, they seem to improve the accuracy of LES tremendously over use of uncorrelated random numbers for inflow turbulence [23].

Second type of synthetic turbulence methods involve generation of spatial modes using analytical functions for inflow disturbances. Among these, the method developed by Batten et al. [24] is based on superposition of sinusoidal modes with random frequencies and wavenumbers, with given moments and spectra. This method, however, is based on a single length scale for characterizing the correlations in all directions. This same length scale also applied to all velocity components. As a result, the spatial structures of the eddies entering the domain may not be fully correct and realization of a truly turbulent state is delayed. Keating and Piomelli [25] used the control planes approach [20] to reduce such delay in establishing an incompressible equilibrium boundary layer. Faster transition may also be possible by specifying the integral lengths in each direction for the three velocity components. The synthetic turbulence method of Sandham and coworkers [26] introduces modes that have (non-sinusoidal) functional dependencies along wall-normal direction to produce near wall streaks in the inner layer and more three-dimensional vortices in the outer layer as observed in boundary layers. Phase information is controlled in this approach but no attempt is made to match statistical moments. This approach tends to generate an unphysical second peak in streamwise fluctuations profile in addition to the near wall peak.

The third method is the digital filtering approach of Klein and coworkers [27]. In this approach random numbers are filtered so that the velocity components are spatially correlated as per prescribed functional forms. Each component has different integral lengths (that characterize spatial correlation) along the three directions. Xie and Castro [28] modified this method by replacing three-dimensional filtering with two-dimensional filtering (on the inflow plane) and correlating the filtered field with its history using an assumed exponential temporal correlation. This approach has subsequently been extended to compressible flows by Touber and Sandham [12]. First and second moments (Reynolds stress tensor components) are matched to prescribed values while perturbations of thermodynamic variables are computed by invoking the strong Reynolds analogy. It is as simple and efficient as the synthetic turbulence method but with slightly better turbulence statistics [12]. A brief description of the technique is provided in Appendix A. It is used here for LES of subsonic and supersonic flows over backward facing steps using a compressible flow solver.

Some inflow generation techniques including the digital filtering approach do not supply solenoidal velocity as required at low speeds. However, the non-solenoidal component of the incoming flow is filtered out using pressure by incompressible flow solvers. The turbulence levels need to recover following an initial dip due to this. When using compressible flow solvers, there is a different problem. Entry of non-solenoidal flow leads to density/entropy fluctuations that are convected with the flow. Depending on the way unsteady pressure and temperature are specified, there could also be density/pressure fluctuations associated with acoustic disturbances which propagate even faster. In addition to checking the efficacy of the compressible digital filtering technique for separated flows using a newly developed compressible LES solver [29], the present study is intended to identify the effects of these fluctuations.

2. Numerical method

A hybrid solver based on the combination of MacCormack and shock capturing SLAU2 schemes is used for integrating the Favre filtered governing equations for compressible flows. The blending of the non-dissipative and dissipative (upwind) schemes is usually done by relying on discontinuity sensors. However, unphysical numerical oscillations tend to persist even far away from discontinuities in solutions obtained using hybrid solvers. So, an additional unphysical oscillation sensor is also used in the present hybrid method to suppress such oscillations. The overall inviscid fluxes are computed as a weighted averages of the fluxes computed using the two schemes. The weight of the upwind scheme is highest near discontinuities and almost negligible in smooth regions of the flow. The weight of the upwind scheme, in addition, also increases monotonically with the amplitude of unphysical two-point oscillations in the density field. The numerical dissipation of the upwind scheme keeps the numerical oscillations under check even away from the discontinuities. The effectiveness of the blending technique based on this additional sensor in eliminating unphysical and undesirable oscillations while ensuring accurate capturing of physical oscillations has been tested by simulating various prototype problems for compressible turbulence and documented earlier [29]. The details are left out here for brevity.

Several sophisticated subgrid models have been developed first for incompressible flows and then extended to compressible flows in last few decades. The differences between predictions of different subgrid models could be significant in temporal simulations but while simulating spatially evolving flows, they tend to be marginal. Flows of interest in engineering fall in the latter category and their predictions depend more on the numerical discretization scheme and the inflow conditions than the subgrid model. For this reason, instead of a complex subgrid model, the Smagorinsky model [30] with van Driest damping of eddy viscosity near walls is used here to compute the subgrid terms that result from filtering of nonlinear advection terms. The cube root of the finite volume cell is used at the filter width while computing the eddy viscosity. The subgrid energy flux term is close by invoking the eddy diffusivity hypothesis and by assuming a subgrid Prandtl number of 0.9.

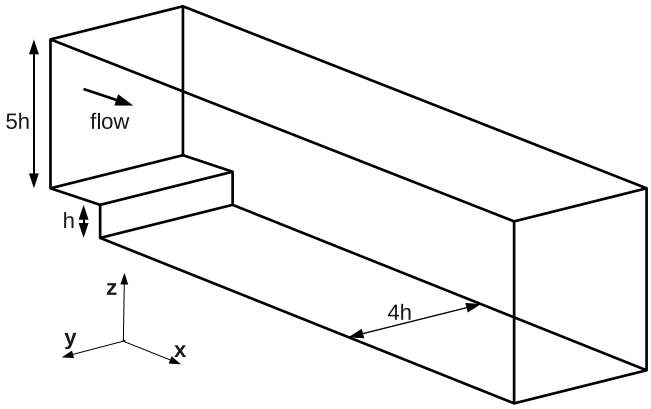

Fig. 1. Domain for LES of subsonic flow over backward facing step. The origin is at the convex corner at the step location. The domain is discretized using a 144 × 72 × 32 mesh similar to one used by Panjwani et al. [31] in streamwise and lateral directions. The near wall mesh spacings in wall units (Y^+) in the three directions near the step are 14, 1.0 and 30 respectively. As the grid is stretched out away from the step and more rapidly close to the exit, the streamwise grid spacing reaches 110.

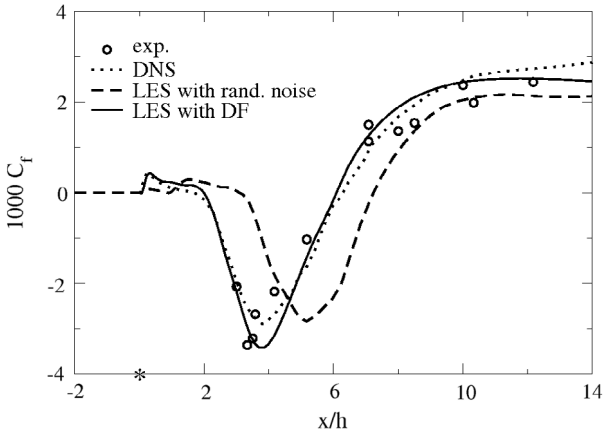

Fig. 2. Friction coefficient on the lower wall. The star symbol corresponds to the step location which is located at the origin.

3. Results

3.1. Subsonic case

The experiment of Jovic and Driver [32], with spatially evolving boundary layers crossing steps on either sides of a channel, has a simple geometry suitable for structured meshes which enable higher order of accuracy than unstructured meshes. This fact and the relatively low Reynolds number help in ruling out lack of resolution as a possible source of inaccuracy. A direct numerical simulation [33] and several LES [23,31,34–40] of it have been reported in the literature. One half of the flow can be simulated due to symmetry about the centerline and the fact that the core flow is uniform and unaffected by the boundary layers. The expansion ratio is 1.2 and Reynolds number based on step height and inlet velocity outside the boundary layer is 5100. The incoming boundary layer is 1.2 times the step height and is resolved using 23 points in the wall-normal direction.

As in most of the past simulation studies, a half of the experiment is simulated. A schematic of the flow geometry is shown in Fig. 1. No-slip boundary and isothermal conditions are used for velocity and temperature, respectively, at the solid walls. Periodic boundary conditions are used in the spanwise (z) direction. A slip condition is used at the top boundary. This does not constitute an approximation since the flow at the center line in the experiment (which is the top boundary in the simulation) has a potential core with flat velocity profile and no turbulence.

A summary of the past LES of subsonic flows over backward facing steps is tabulated in chronological order in Appendix B. Prediction of recirculation zone characteristics, especially its length, is often considered a measure of LES accuracy. How it varies with Reynolds number and expansion ratio is discussed elsewhere [41,42], the discussion here is confined to its numerical prediction. Since inlet turbulence is one of the main issues in this study, the inflow conditions used and the resulting predictions of the reattachment length are listed in addition to details of flow geometries, conditions and grids. The experiment of Jovic and Driver [32] is the most simulated and can be considered a benchmark test case for low speed LES capability. The following major observations can be made.

1. The flow has a combination of large structures generated due to instability of the shear layer formed at the corner and small scale turbulence [33,36]. The large scale structures generated due to shear layer instability survive well past the reattachment point but breakdown eventually [33,43,44]. The formation and breakdown of the large structures need to be captured accurately. If random noise is added to the mean flow to approximate turbulence, much of it is wiped out by numerical or physical dissipation and what remains is not very effective and reattachment shifts to a downstream location [23,31,45].
2. When the approaching boundary layer is fully turbulent, numerical resolution and accurate inflow conditions are more important than the subgrid closure [31,37,46]. Transition (physical or numerical) predictions do vary from one subgrid model to another [36,39,42].
3. Inflow conditions drawn from a precursor LES are ostensibly the most accurate but they need to be specified sufficiently upstream of the step. The separated shear layer dynamics do influence the flow upstream of the step. The inflow boundary should be sufficiently upstream so that it is outside the zone of influence. Forcing the inflow conditions from a precursor LES at a location close the step would likely lead to errors downstream and this may be the source of error in some of the LES that used precursor simulations.
4. Flows over backward facing step become independent of inlet conditions if the streamwise coordinate is scaled with the predicted reattachment length [31], a fact that is consistent with experimental findings [47]. The same dynamics are played out over a longer distance even if the shear layer breakdown is delayed. The profiles of first and second order statistics from almost all simulations of Panjwani et al. were nearly identical [31] and also match with corresponding experimental and DNS [33] predicted profiles at non-dimensional streamwise locations. In a way, they obviated the need for accurate inflow conditions while verifying LES capability and established that their mesh provides sufficient resolution for LES of this flow.
5. To reduce the computational cost associated with the use of a compressible flow solver, a higher Mach number (∼0.3) has been used in the some simulations. Compressibility effects, though higher than in the experiments, have been assumed to be negligible [23,35,38].

A 144 × 72 × 32 mesh similar to one used by Panjwani et al. [31] along streamwise and lateral directions is used here for LES at Mach number of 0.1. The inlet and outlet boundaries are 2.5 and 20 times the step height, respectively, away from the step location

just as in their study. This is done deliberately in order to facilitate comparison on as similar terms as possible. While inflow boundaries were placed about 10 step heights ahead of the step in few LES studies [23,34,38,48], many other LES studies [15,35,43,44,49] with spatiotemporally correlated inflow conditions placed in the inflow boundary 1–4 step heights ahead of the step. The wall-normal grid spacing near no-slip walls is such the y^+ (calculated based on asymptotic value of friction coefficient, C_f along the axial direction) is below unity. In the spanwise direction, higher number of points are used instead of the 20 points in their study. In wall units, spanwise grid spacing is 30, while axial grid spacing varies between 14 and 110 (average is 37). In comparison, the DNS [33] was conducted using a $768 \times 192 \times 64$ mesh with wall-normal grid spacing about 0.3 wall units. The computational domain, however, starts 10 step heights upstream of the corner. Due to use of randomized phase angles in prescribing inlet turbulence, statistical characteristics were found to quickly drift away and then slowly approach their corresponding targets. Other than the longer inlet portion, all other dimensions are nearly similar in DNS [33] and present LES.

As in case of DNS [33] , flat plate turbulent boundary layer profile [2] is used to specify the mean velocity profile at the inlet. The fluctuating quantities are specified using the digital filtering approach. For comparison, a simulation is also performed with randomly fluctuating unsteady velocity components without any spatio-temporal correlations.

The second order statistics of velocity fields within boundary layers are known for a range of Reynolds numbers (e.g., [2]) and can be used to scale the digitally filtered unsteady velocity components. The length scales needed to determine filter widths and weights needed to correlate the inflow turbulence in time have to be specified. Precise spatial variations of integral lengths associated with two-point velocity correlations with in boundary layers are unknown. Klein and coworkers [27] have warned against the use of strongly varying scales for digital filtering. Their original implementation relied on uniform length scales. Veloudis and coworkers [50] used piece-wise constant levels to account for wall-normal variations of length scales for LES of periodic hill channel flow in which flow separates and reattaches on the downstream side of the hill. Their results including second order statistics, however, were quite similar when compared to those generated using uniform length scales. The differences were mainly in the near wall streamwise velocity fluctuation levels in the recovery region. Xie and Castro [28] used uniform length scales for cross stream directions but their streamwise length variation was similar to that of the streamwise velocity so that the weights for correlating the inflow in time were uniform. Their work also confirmed the relative insensitivity of the results to nearly 30% variations in nominally prescribed length scales.

Touber and Sandham [12] listed the digital filter coefficients for LES of a supersonic boundary layer but they are not used here for following reasons. First, the filter widths are specified in terms of number of points. The transverse length scales would, therefore, vary roughly the same way as the wall-normal grid spacing without regard to the actual physical correlation lengths. The number of grid points here is quite low and the grid stretching is higher than in their simulation. If the numbers they prescribe are used to determine the points used for filtering, especially for the transverse length scales, the actual length scales end up being much higher than the boundary layer itself. Touber and Sandham also noted that the digital filtering is relatively independent of filtering coefficients as long as the prescribed length scales are at least as large the integral length scales of the flow.

Based on these observations from literature, the original idea of uniform length scales is adopted here. The length scales along streamwise, wall-normal and spanwise directions as fractions of incoming boundary layer thickness are 1.2, 0.35 and 0.8 respectively. Along a given direction, the same filter is used for all three velocity components as in the work of Xie and Castro [28].

Further increases in streamwise and spanwise lengths (by even 50%) do not alter the results significantly. The only simulation that could not produce accurate results was one with transverse length below 0.2 as a fraction of boundary layer width. Compared to prior studies [12,28], the spanwise length scale used here is quite high. Reduction in spanwise correlation length would not make sense given that only 32 points are used in this direction. Any reduction would lead to generation of eddies that are very poorly resolved in this direction. In the context of relative insensitivity of the predictions to the prescribed length scales, it is to be noted, as Keating and Piomelli [25] pointed out, that establishing equilibrium boundary layers (in channel flows and on flat plates) with no shear layer instability mechanisms is more stringent test for inflow generation techniques than the present test case where the post step dynamics are mostly dependent on the shear layer as long as it is triggered adequately.

The digital filtering nevertheless cannot overcome one artifact when using a compressible flow solver. The incoming turbulence is not solenoidal and as a consequence, density fluctuations are introduced into the flow that seem to persist all the way to the exit.

The predicted streamwise variations of the skin friction coefficient are shown in Fig. 2. The reattachment point for the primary recirculation zone predicted with digital filtering turns out to be at $6.09h$. The experimental value is between $6.0h - 6.1h$ and the DNS [33] prediction is $6.28h$. Going by reports in literature, the distance between the inflow boundary and the step in present simulations is much smaller than the distance needed to establish an equilibrium boundary layer using digital filtering. However, the digital filtering seems to generate an energetic broadband spectrum including eddies that can trigger the Eigenmodes of the shear layer and smaller eddies that help in the breakup of large vortical structures. Still, a more accurate prediction than that of DNS [33] is perhaps just happenstance.

As in past LES studies based on use of random noise for approximating inlet turbulence [23,31,45], the recirculation length is significantly overpredicted. In past LES where large eddies that can trigger the instability are present either due to use of a presimulation or synthetic turbulence, the predictions of the reattachment length generally turn out to be lower and closer to experimental values. While use of a precursor simulation can be expected to lead to more accurate predictions, that does not always seems to be the case. LES performed this way [34,35,43,44,46,49] end up with larger errors than when stochastic turbulence [23,38], synthetic eddy method [15] or digital filtering (present work) techniques are used for prescribing synthetic turbulence. Aider and Danet [35] speculate that the reattachment length, which is already underpredicted when using random noise, falls further when precursor simulation is used instead for specifying inflow fluctuations due to the use of outflow boundary conditions instead of slip boundary conditions at the top wall. Their simulations correspond to an infinite expansion ratio and reattachment length has been shown [41] to increase with expansion ratio. Obviously, further work is needed for a proper explanation.

The large scale structures generated due to shear layer instability survive well past the reattachment point. Evidence for this was provided in the earlier studies [33,43,44] by plotting the temporal profiles of the instantaneous spanwise-averaged reattachment point location and pressure slightly above the mean reattachment point. The same is done here in Fig. 3. The spanwise-averaged pressure fluctuates rapidly and so additional moving time-window (corresponding to about 40 time steps) averaging is also done to filter out high frequencies. Note that the number of points in spanwise direction and the time step used for numerical integration are much lower here than in case of DNS [33].

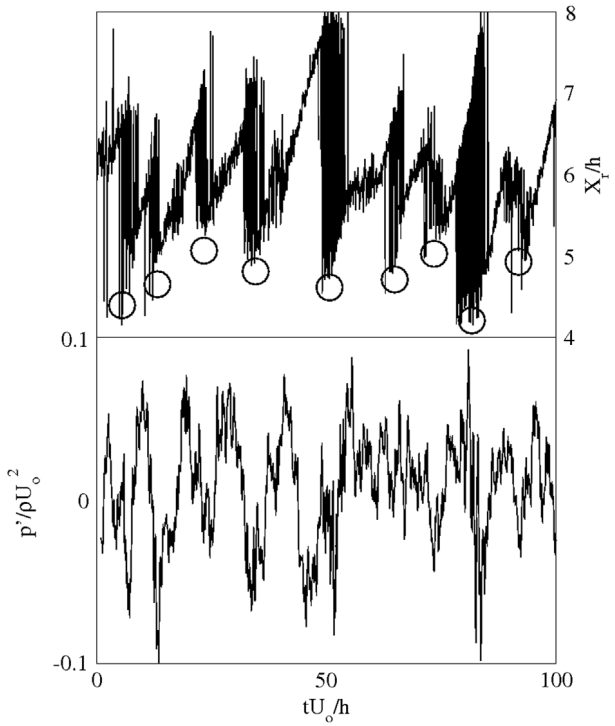

Fig. 3. Spanwise averaged instantaneous reattachment point location (X_r), and non-dimensional spanwise and time-window averaged pressure fluctuation (p') at $0.25h$ above mean reattachment point location are plotted with non-dimensional time at top and bottom respectively. Circles indicate shifts in reattachment point due to a large vortex passing by the mean location. Most of the shifts are sudden while two of them are more gradual. ρ and U_o are inflow density and mean inflow velocity outside the boundary layer.

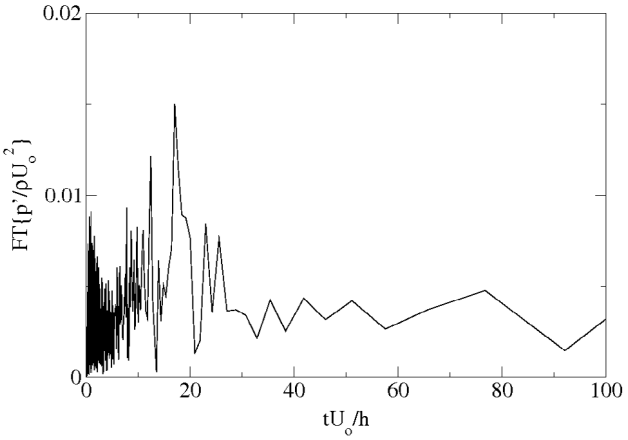

Fig. 4. Fourier transform of pressure fluctuation shown in previous figure.

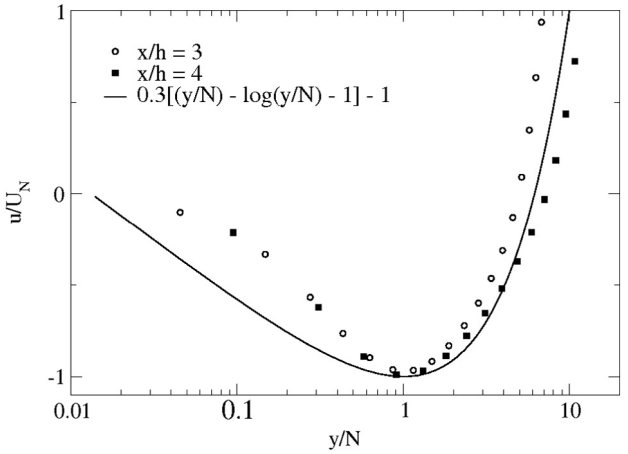

Fig. 5. Comparison of velocity profiles in primary recirculation zone with Simpson's model [51].

The sudden drops in reattachment length are due large and mostly two-dimensional structures passing by the mean location. The dips in pressure profiles at time instances near these drops confirm this hypothesis. Fig. 3 clearly indicates seven large scale structures passing through while evidence is a bit weaker for two more. The Strouhal number characterizing the shedding of the large structures passing is, therefore, inferred to be between 0.07 and 0.09. Alternative to this is the computation of Fourier transform of the pressure data. This transform is plotted with time period (non-dimensionalized using step height and reference velocity) as the abscissa in Fig. 4. The time period corresponding to the largest peak is near $17h/U_o$ which is also the prediction from DNS study [33].

Aider and Donat [35] have shown that the upstream turbulence specification affects the vortex shedding frequency. In addition to the reattachment length, the Strouhal number is also well predicted by using the digital filtering approach here . Their LES predicts that the Kelvin–Helmholtz vortices breakdown almost immediately if a precursor simulation is used for inflow turbulence while they remain two-dimensional if random noise is used instead. The present analysis, however, shows that fairly large coherent structures survive well past the mean reattachment location in the present LES. Agreement with DNS [33] in terms of structural aspects of the flow provides additional confidence in present predictions.

The LES overpredicts the length of the secondary recirculation bubble slightly. It ends at $2.07h$ away from the corner in present LES as compared to about $2.5h$ in past studies which have noted this information [34,40]. The location values are $1.6h$ and $1.7h$ in experiments [32] and DNS [33], respectively. Even smaller bubble of size 0.042 h is predicted at the corner in DNS. The LES with digitally filtered inflow conditions predicts its size to be 0.072 h which cannot be expected to be accurate given that it spans less than four grid points in axial direction. Within the recirculation zone, flow is not fully turbulent and the viscous sublayer and log-layer scaling cannot be expected. Simpson [51] suggested the following empirical scaling law for regions well with in the recirculation zone that was verified using DNS [33] data at locations $2h$, $3h$, $4h$ and $5h$ away from the corner.

$$\frac{u}{|U_N|} = 0.3\left[\frac{y}{N} - log(\frac{y}{N}) - 1\right] - 1 \tag{1}$$

N in this equation is the distance between the wall and location of maximum negative velocity (U_N).

In case of LES, the location $2h$ distance away from the corner along the bottom wall is near the zero shear stress point (where the secondary bubble ends) and this scaling likely does not hold. So, locations $3h$, $4h$ away from the corner are chosen for verification of this scaling. Fig. 5 shows that the profiles at these two locations are as close to this scaling law as the DNS predicted profiles [33].

Four axial locations are chosen for comparison of the velocity profiles. One is well within the recirculation zone, second is at the reattachment point and other two are in the recovery zone. Experimental data is available at locations $4h$, $6h$, $10h$ and $15h$ away from the corner.

Westphal and Johnston [47] suggested that flow statistics have a universal nature with respect to a normalized coordinate $X^* = (x - X_r)/X_r$, where x is the axial coordinate and X_r is the axial

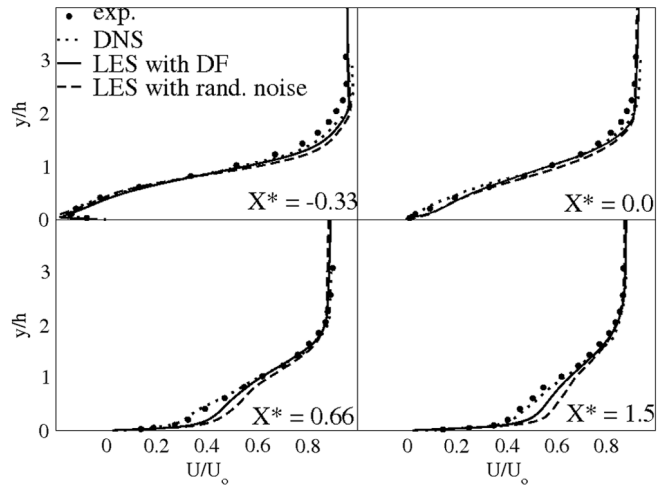

Fig. 6. Mean streamwise velocity profiles at various locations.

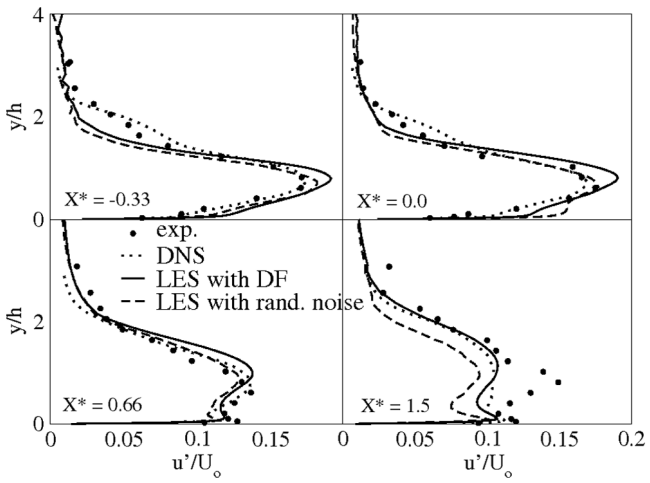

Fig. 8. Profiles of streamwise velocity fluctuations.

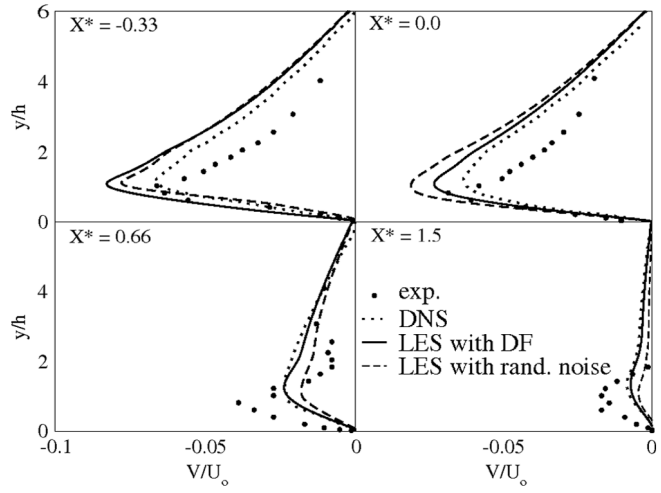

Fig. 7. Mean cross-stream velocity profiles at various locations.

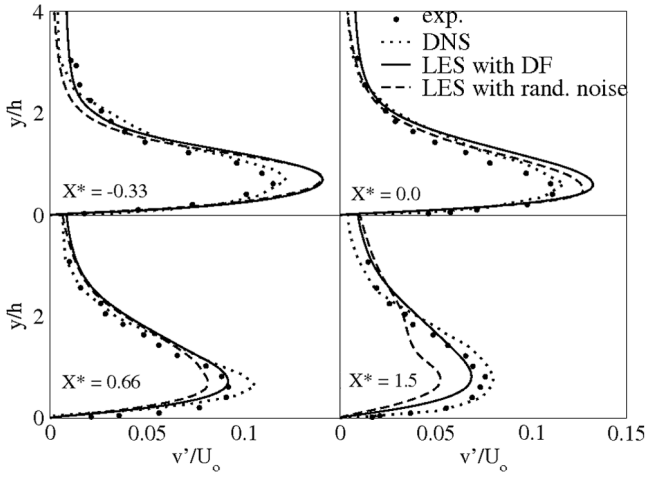

Fig. 9. Profiles of cross-stream velocity fluctuations.

location of the average reattachment point. This suggests that the shear layer dynamics follow the same physics expect that they are stretched out over a longer length in cases where the triggering is not proper. This hypothesis, confirmed in some of the past LES studies [31,35,45], allows for comparison of statistics from various simulations/studies even if their reattachment point predictions are different. In terms of scaled coordinates, the experimental [32] and DNS [33] data are available at approximate X^* locations of −0.33, 0.0, 0.66 and 1.5. The mean velocity predictions from the LES simulations at these locations are compared to DNS [33] predictions and experimental data [32] in Figs. 6 and 7. There are slight deviations from experimental data and DNS [33] predictions at the two downstream locations as in other LES studies [31,48]. With in the recirculation zone, the transverse velocity predictions of DNS [33] and LES depart from the experimental data [32]. The predictions are closer to each other and so it is likely that this deviation is due to experimental error. The deviation is about 2% of mean free stream velocity. The experiments [32] were conducted using a free stream velocity of 7.72 m/s and so in absolute terms, it is only about 0.15 m/s which could very well be with in the error margin of the instrument.

The scaling used in these plots is of little consequence when comparing predictions of DNS [33], present LES with digital filtering with experimental data since X_r values in all three cases are very close. The comparisons are just as good if same physical coordinates are picked instead of the same scaled coordinates. In case of LES with random turbulence, the axial location for a given X^* is further downstream of the corresponding physical location in the experiment.

The second order statistics from simulations here are compared to DNS [33] predictions and experimental data [32] in Figs. 8–10. Note that these statistics correspond to root-mean-square values of filtered velocity components. Subgrid component of the velocity fluctuations are not considered.

The LES predictions compare well with experimental data with couple of exceptions. First, the turbulence levels (especially u') are underpredicted at first two upstream locations around $y/h \sim 2$ (above the recirculation bubble). The higher values in experiments [32] and DNS [33] are due to convection of turbulence in the fully developed incoming boundary layer past the step. The inlet boundary is far more distant from the step location in the DNS [33] than in case of LES. The ratio between this distance and the boundary layer thickness is nearly 10 in case of DNS [33] while it is only around 2 in case of LES. Though digital filtering introduces fluctuations that have desired second moments and are spatio-temporally correlated, convection over 2 boundary layer widths is not sufficient to result in correct phase information. This leads to lower fluctuations within the boundary layer at the step and

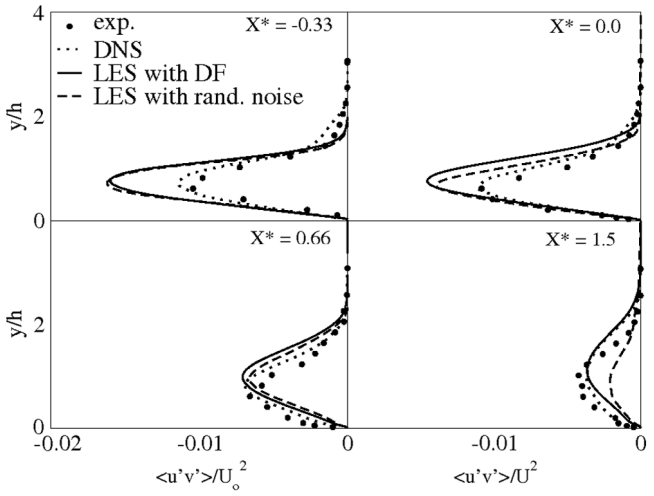

Fig. 10. Reynolds stress profiles.

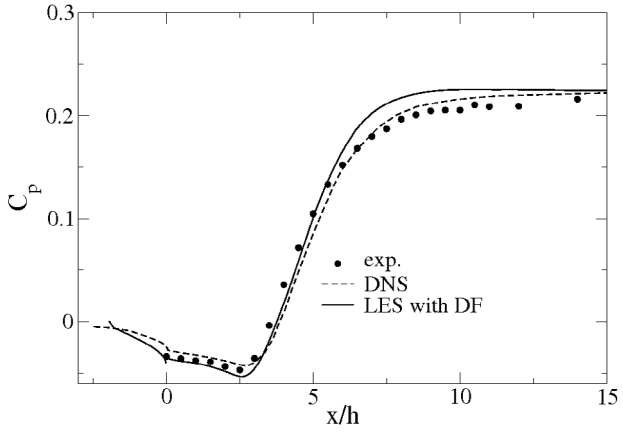

Fig. 11. Pressure coefficient variation along the bottom wall.

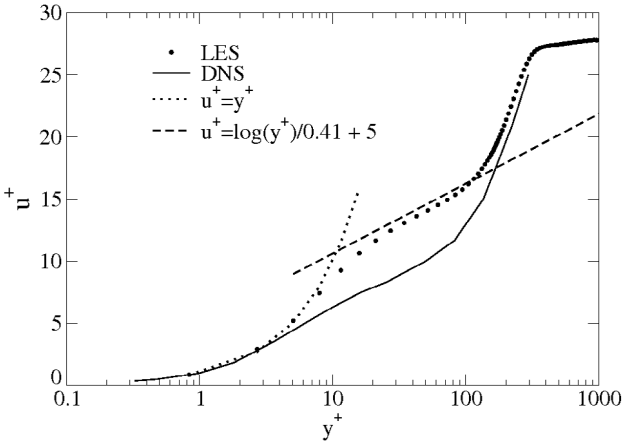

Fig. 12. Mean velocity profiles in wall coordinates.

locations above the shear layer. Similar deviations are found in LES of Kanchi and coworkers [38] despite using a stochastic model for inflow turbulence specification about 10 step heights ahead of the step. The deviations are obviously higher in LES with random inlet turbulence [36,39] even when a relatively long inlet section is used [39]. The LES of Benocci and coworkers [34] does not have this problem since they used a concurrent presimulation to generate an equilibrium boundary layer which was then followed by about 11 step heights of flow path before the step. In the recovery region, u' profile predicted using the digital filtering approach is close to one predicted using DNS [33] but the two profiles deviate from experimental data [32] likely due to experimental error. Note that DNS [33] prediction is almost a faithful representation of the experimental flow field. The fluctuation levels drop off much more rapidly in this region in the case with random inflow turbulence which could be explained as follows. The predicted reattachment length is much higher in this case ($> 7.2h$) and so the location $X^* = 1.5$ corresponds to axial coordinate that is nearly 18 step heights away from the step where grid is stretched rapidly to create a sponge layer to prevent problems associated with reflections from unsteady outflow. This high level of stretched obviously leads to damping of fluctuations.

With in the recirculation zone, LES predictions of peaks Reynolds shear stresses are more negative than in the experiments [32] and in the DNS [33]. The deviations are almost 40%. The errors are, however, small in absolute terms though they seem high on a relative basis. Any significant error in the transverse Reynolds stress profile would lead to noticeable error in the mean axial velocity profile. From Fig. 6, the mean velocity profiles predicted by LES match with corresponding DNS [33] predictions and experimental data [32] at these locations.

Many LES of this flow [31,34] reported in literature predict Reynolds stress profiles closer to DNS [33] profiles (at least in the scaled coordinate system suggested by Westphal and Johnston [47]) with the exception of the LES conducted by Kanchi and coworkers [38]. This LES is, in a way, similar to one with digital filtering here. It was based on a stochastic technique of Gao and Mashayek [21] for generating temporally correlated inflow turbulence which is functionally similar to the digital filtering technique used here. They also used a compressible flow solver and to reduce computational cost, the inlet Mach number was set to 0.2. At higher Mach numbers, the effects of dilatation due to compressibility are expected to be higher. This and both LES in present study seem to point to an increase in Reynolds stress as one such effect.

Near the outflow boundary, the axial resolution is very coarse with axial grid spacings close to the step height. This, in combination with the approximations associated with the Smagorinsky subgrid model and the outflow boundary conditions, start to affect the accuracy of solutions at axial locations beyond $14h$ distance away from the step location. The friction coefficient levels off much sooner in LES while it continues to vary even at the exit in the DNS [33]. This is the case in LES of Benocci and coworkers [34] although to a lesser extent. Due to overall delay of dynamics in the streamwise direction, the simulations of Panjwani and coworkers [31], on the other hand, predict strongly varying friction coefficient close to the exit.

The bottom wall pressure coefficient profiles are compared in Fig. 11. Pressure also levels off closer to the corner in LES while it is still varying slowly at the exit in DNS [33]. LES predicted axial velocity profile at $10h$ distance away from the corner is plotted in wall units in Fig. 12 along with corresponding DNS prediction. Profiles in both viscous and log-layers are close to the scaling laws expected of equilibrium boundary layers. By comparison, the DNS [33] predictions are comparatively farther away from these scaling laws. Even though the friction coefficient seems to flatten out around 15 step heights downstream of the step in LES of Benocci and coworkers [34], the mean velocity deviates from the equilibrium wall scaling laws (as in DNS [33]). Their wall-normal and spanwise resolutions are nearly the same as in the present case while their axial resolution is much finer. The very coarse resolution in the present simulation may be damping out the large scale

structures generated by the shear layer. The presence of these large structures is the likely reason why the mean velocity in DNS [33] departs from the equilibrium wall layer scaling laws. The evolution of these large 2-dimensional structures (which have been argued to exist using Fig. 3), their breakdown due to turbulence are well captured in DNS [33], while the present LES which has an axial grid spacing of almost half the step height at this location cannot be expected to do that. The LES predictions of pressure recovery and near wall mean velocity behavior are expected to be better with higher grid resolution especially in the axial direction closer to the exit.

Density fluctuations generated with in the boundary layer at the inflow plane do not decay and are convected into the recirculation zone. The fluctuations in the instantaneous density field have an amplitude around 3% in this zone when digital filtered inflow conditions are used while they are lower than 2% when using random noise to approximate inflow turbulence. They do not seem to adversely affect the overall dynamics or the prediction of second order turbulence statistics since they are in line with expectations for the mesh resolution used.

3.2. Supersonic case

Supersonic flows past backward facing steps are encountered in some of the scramjet combustor designs. The separation zones that form behind the steps are mainly useful in fuel-air mixing and anchoring of flames. Though a few experimental studies of such flows including some which also have injection into the separation zone have been conducted, detailed characterizations of the turbulence like second order moments like in case of subsonic flows are, to authors' knowledge, are not available in open literature. Perhaps this is why only a few LES of these type of flows have been attempted [52,53]. Only one by Ayyalasomayajula and coworkers [54] has reported second order statistics. Their results are also likely free of uncertainties associated with inflow conditions since they were specified using a precursor simulation of flow through a converging-diverging nozzle. This study is used as a reference for the present one.

The flow parameters are listed in Table 1. The Reynolds number based on step height and inflow quantities outside the boundary layer is roughly 2.8×10^5. With incoming boundary layer as the reference length, it is roughly 9×10^4. A cartesian mesh is clustered using hyperbolic tangent functions near solid walls.

The LES of Mach 2 flow over a backward facing step reported by Liu and coworkers [53] are based on very coarse meshes (less than one-tenth the number of points used here) and inviscid fluxes are computed using a Riemann solver extended to second order accuracy using a MUSCL scheme. Such schemes can capture shocks very effectively but are too dissipative to capture turbulence dynamics and are not really suited for LES. The Reynolds numbers based on step height in LES of Ishiko and Shimada [52] is 1.9×10^5. Its value based on boundary layer thickness is 19000. They used a $200 \times 76 \times 400$ non-cartesian mesh. The mesh here seems relatively coarse given that the Reynolds number based on boundary layer is about 5 times higher. However, the computational domain is much smaller, about $10h \times 5h \times 2h$ here as compared to their $40h \times 15h \times 2h$. The difference is even more stark when viewed in boundary layer terms.

Compared to the meshes used for LES of boundary layers flowing over expansion–compression corners [9,55], the mesh used here is relatively coarse. The flows in such geometries expand more gradually and separate on the ramps rather than at the expansion corner. Otherwise, they have essentially the same dynamics as the flows over backward facing steps. The flow over a step is a particular case when the ramp angle is 90^o. These past LES performed for a ramp angle of 25^o also have ramp height to boundary layer ratio of 3.0 which is same as the step height to boundary layer ratio here. The overall grid points in both of them are nearly the same as in the present LES (about 2.4 million) but their computational domains are much smaller in lateral and spanwise direction (roughly 6δ&2δ compared to 15δ&6δ in present LES). The Reynolds number based on boundary layer width is also 5 times higher in case of present LES. To provide sufficient resolution near solid walls, the grid here is stretched out rapidly near the top and outflow boundaries. This also helps in creating a numerical buffer zone which prevents contamination of the flow field due to disturbances at the outflow boundary. Also, the grids for the expansion–compression geometry need to be clustered in the axial direction near both corners, while in the present geometry, it is clustered only at one axial (step) location. The first cell is located about 2.6 wall units away from the wall in the transverse direction. The grid spacings in streamwise direction range from 11 to 60 wall units while spanwise grid spacing correspond to about 26 wall units. Given the mesh used, the present simulations can be considered very large eddy simulations. The implications of this fact are discussed later.

Table 1
Parameters used for LES.

h (step height)	6.35 mm
Domain size	$9.5h \times 5h \times 2h$
Mesh size	$240 \times 140 \times 64$
M (Mach number)	1.5
Total pressure	3.72 bar
Total temperature	300 K
Inflow boundary layer thickness	2.0 mm

Fig. 13. Instantaneous density (units : kg/m^3) field in LES based on digital filtering technique for inflow specification.

The correlation lengths needed for determining the filter coefficient relative to incoming boundary layer thickness are retained to be the same as in the subsonic case except for the wall-normal length scale (as a fraction of boundary layer thickness) which is increased to 0.6.

The mean velocity profile at the inlet is taken from the reference study. Profiles for a Mach 1.7 turbulent boundary layer in Morkovin's form provided by Touber and Sandham [12] are used here for prescribing second order moments in the digital filter. Reynolds stresses in this form are nearly independent of Mach number [12] and so there is no significant error is incurred in using this data for the present Mach 1.5 boundary layer.

The density field predicted using digital filtering for inflow specification is shown in Fig. 13. Density fluctuations can result from entropy fluctuations resulting from a non-solenoidal nature of the incoming velocity field or from acoustic fluctuations. As explained earlier, the pressure in incompressible flow solvers ensures that non-solenoidal component of the incoming flow is filtered out and since there is no spatially dependent thermodynamic pressure in such formulations, digital filtering leads to purely vortical

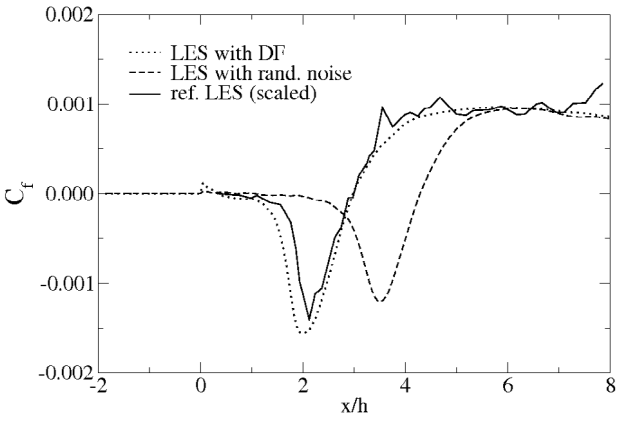

Fig. 14. Skin friction coefficient along the lower wall.

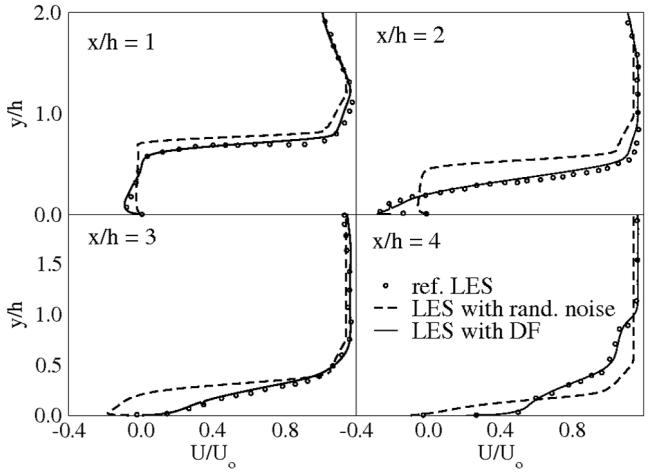

Fig. 15. Mean streamwise velocity profiles at various locations.

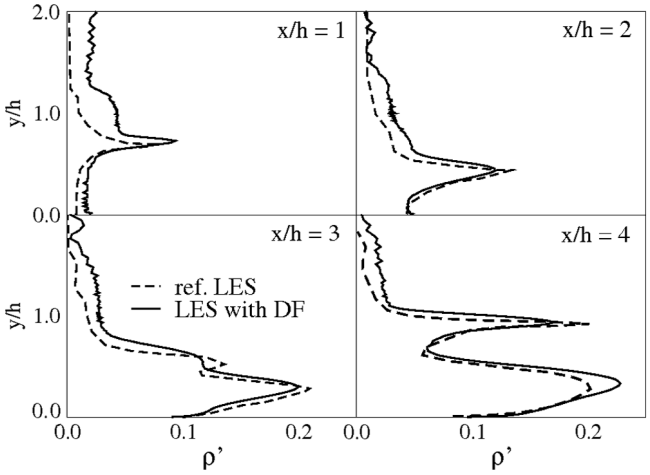

Fig. 16. Profiles of density fluctuations at various axial locations.

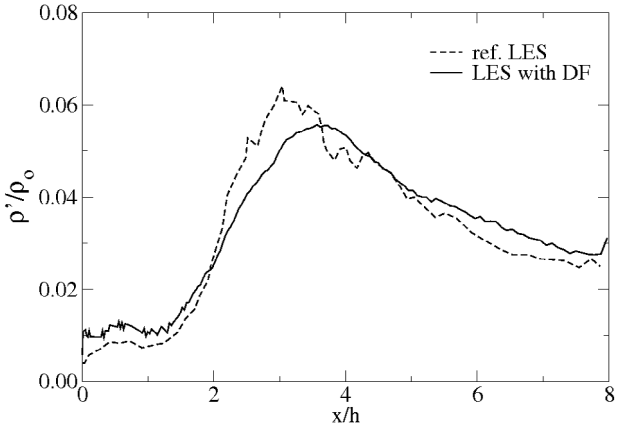

Fig. 17. Variation of density fluctuations along the lower wall.

disturbances in the boundary layers. In compressible flow solvers, the entropy and acoustic fluctuations propagate into the flow. The acoustic fluctuations at a given location propagate into its domain of influence which may extend out of the boundary layer. Such fluctuations starting from the inlet plane itself propagate outside the boundary layer along Mach lines and contaminate the expansion fan and flow further downstream. This feature is also evident in numerical schlieren images generated in DNS of supersonic flows over an expansion ramp [56] based on digital filtered inflow conditions. The LES of such flows using recycling–rescaling method does not seem to have this problem. Roidl and coworkers [18] used a sponge layer [16] close to the inflow plane to reduce the unphysical acoustic oscillations generated by synthetic inflow specification. The present work was done without the knowledge of this approach. It can probably be applied to all synthetic turbulence specification approaches to avoid contamination downstream.

The flow, as in the experiment, seems to reattach roughly 3.0h downstream of the step location. When uncorrelated random numbers (scaled to produce specified intensity profiles) are used for specifying inflow turbulence, as in the subsonic case, the reattachment point shifts downstream to a point more than four steps heights away from the corner.

Predicted variations of skin friction coefficients along the lower wall downstream of the step are plotted in Fig. 14. The prediction of Ayyalasomayajula and coworkers [54] shows a similar variation but the values they reported are far too low ($O(10^{-4})$) perhaps due to a scaling error. The profile they predicted has been scaled and included in this figure. Though they state that the reattachment point in their calculation is about 2.8 h downstream of the step location, the location that can be inferred from the friction coefficient plot turns out to be 2.99 h downstream of the step which is closer to the experimental location 3 h from the step. The locations predicted by LES with and without digital filtering turn out to be 2.98 and 4.27 step heights downstream of the step, respectively.

Comparison of first and second statistical moments are made at four different locations. First two are well with in the recirculation zone, third is at the reattachment point and fourth is further downstream. The mean velocity predictions are compared in Fig. 15. The results from the present LES match well with those from reference LES when only when digital filtering is used.

Unlike in the subsonic case, the mean velocity profiles resulting from the two LES at a given non-dimensional axial location (using predicted reattachment length as a reference) do not match, especially, if the location is at or beyond the reattachment point. This is because, in addition to shear layer dynamics and expansion, there is an additional effect of the shock in the supersonic case. The predicted shock inclinations and strengths are quite different. So, the self-similarity does not seem to be applicable beyond the recirculation zone.

The profiles of density fluctuations at the four axial locations are shown in Fig. 16. The profiles are mostly similar to ones predicted by the reference LES, but in the expansion fan (first two

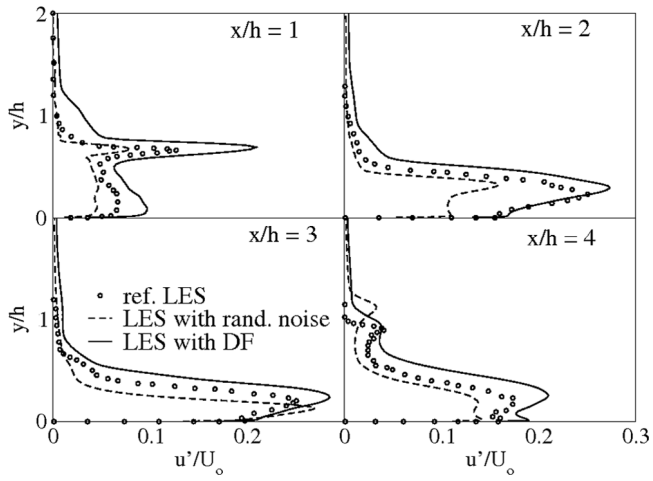

Fig. 18. Profiles of streamwise velocity fluctuations at various locations.

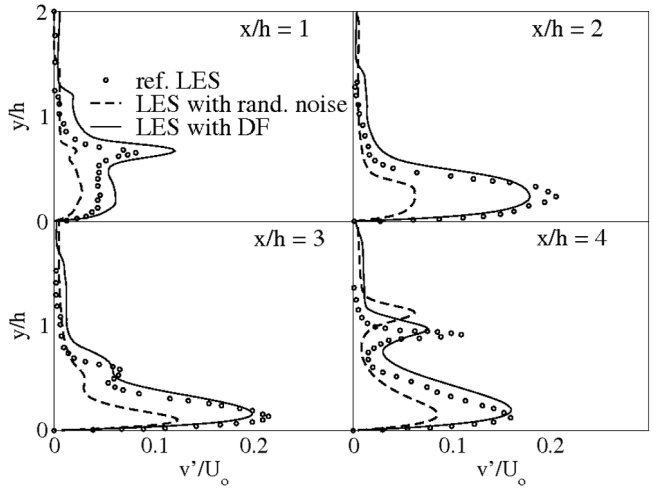

Fig. 19. Profiles of cross-stream velocity fluctuations at various locations.

upstream location), the present LES predicts much higher density fluctuations due to the presence of acoustic disturbances generated at the inflow boundary. Perhaps as a consequence of increased density/entropy fluctuations, the peak in density fluctuations associated with the oscillations of the slip line at the first axial location is also overpredicted as a result of these disturbances. It is to be noted here that the simulations for present work were conducted with being aware of very important work of Roidl et al. [18]. A sponge layer selectively used to damp out unphysical acoustic fluctuations generated by inflow specification was found to reduce almost completely the contamination of results downstream and would probably be needed for almost all synthetic turbulence specification approaches. At the last location, the peaks associated with shock fluctuations are much closer to each other.

The density fluctuations on the lower wall are plotted in Fig. 17. In the reference LES, the fluctuations peak almost at the reattachment location while in the present LES, the peak is shifted slightly downstream.

The predicted velocity fluctuations are plotted in Figs. 18 and 19. The near wall peaks in streamwise fluctuations are higher and away from the wall in the present LES which typically indicates the need for better resolution of near wall dynamics. Note that the grid used here is very coarse for the Reynolds number of the flow. The larger peak at the first axial location is associated with the fluctuations of the slip line. As pointed out in the discussion related to density fluctuations, the slip line oscillates more vigorously due to the unphysical noise generated at the inflow boundary. Above the slip line also, the present LES predicts higher density fluctuations (around $y/h \sim 1$). In the reference LES, surprisingly, there do not seem to be any velocity fluctuations just above the slip line. The fluctuations with in the boundary layer (which is about one-third the step height) upstream of the step should be convected along with the flow. The profile predicted by the present LES above the slip lines is typical of the boundary layer velocity fluctuations profile above the near wall peak. The velocity fluctuations, unlike the density fluctuations, die out at nearly one-third step distance away from the slip line. This reflects roughly the size of the upstream boundary layer.

There is generally a better match between the predictions of the two LES in case of cross stream fluctuations as compared to stream wise fluctuations. In Fig. 19 also, there is evidence at the first axial location for convection of boundary layer turbulence along the slip line. At the most downstream location, there is a peak in cross stream fluctuations resulting from oscillations of the shock wave. A broader and lower peak in the present LES indicates the need to resolve the shock more crisply.

4. Conclusions

Digital filtering technique developed originally by Klein [27] and extended to compressible flows by Touber and Sandham [12] is used to generate inflow conditions for both subsonic and supersonic flows over backward facing steps. The spatiotemporal correlations that result from filtering lead to generation of well resolved eddies of various sizes that can be expected in realistic boundary layers. The characteristic modes associated with shear layer instability are easily triggered just as in case of a realistic boundary layer crossing a step. The size of the recirculation zones and their internal dynamics are also accurately predicted as a result. Skipping the filtering step, on the other hand, results in high frequency oscillations that can easily be damped out by viscous/subgrid stresses or numerical damping. Due to the weaker triggering of the instabilities, the shear layer dynamics are stretched out over a longer region of space. This results in longer recirculation zones than in the experiments. The overprediction of the primary recirculation bubble size is more drastic in case of supersonic flow.

The present work is consistent with Westphal and Johnston [47] observation that the dynamics of the shear layer and the recirculation zone formed created by subsonic flow past a backward facing step are relatively unaffected by inlet conditions if the streamwise coordinate is scaled by the reattachment length. Separation zones are most often used to stabilize flames in combustors. Given the space constraints in combustors, accurate prediction of reattachment length is highly necessary. Based on past [31,33,39] and current studies, it is clear that next to numerics, proper inflow specification is a key requirement for accuracy and the digital filtering technique provides a relatively simple way of doing that. Smagorinsky model [30] is generally good enough and use of more sophisticated subgrid models do not lead to much improvements in accuracy [31,39].

Inflow turbulence seems more important in supersonic flows for a couple of reasons. There is no self-similarity based on coordinate transformation like in the incompressible case. This is due to the fact that reattachment shock strength depends on the location of the recirculation zone. Therefore, the predictions of the size of this zone is very important. While prediction of recirculation zone size vastly improves with use of the digital filtering technique in supersonic case also, the unsteadiness in the supersonic region of the inflow boundary creates unphysical noise that is propagated

Table 2
LES of subsonic flows over backward facing steps reported in past literature.

Ref.	Conditions, mesh	Inflow BC	X_r (X_r exp.)	Comments
Marrano et al., 2001 [42]	ER:1.67, Re_h:11000, Grid : 230 × 56 × 72 Structure function (SF), dynamic Smagorinsky (DSM) , dynamics mixed (DMM) LES models	Laminar inflow (as in exp.)	SF : 6.0 (7.0) DMM : 7.1 (7.0) DSM : 7.2 (7.0)	DSM and DMM overpredict and underpredict u' respectively.
Avancha & Pletcher, 2000, 2002 [43,44]	ER:1.5, Re_h:5540, Grid : 72 × 45 × 48 (post-step), Dynamic Smagorinsky (Germano's subgrid model)	Interpolated from LES of fully developed channel flow and introduced $x = -$h	6.1 (6.51)	u' and v' are overpredicted slightly in the recirculation zone
Benocci et al., 2005 [34]	ER:1.2, Re_h:5100, Grid: 116 × 58 × 32 (post-step), Smagorinsky model constant = 0.1	Interpolates from LES of boundary layer and introduced at $x = -11$h	6.6 (6.1)	u', v' overpredicted near reattachment and downstream locations
Dejoan et al., 2005 [49]	ER:1.5, Re_h:3700, Grid: 96 × 80 × 32 (post-step) Smagorinsky , WALE models	Interpolated from LES of fully developed channel flow and introduced $x = -4$h	7.0 (6.0*)	Reynolds stress slightly underpredicted with recirculation bubble, u', v' not shown
Saric et al., 2005 [46]	ER:1.5, Re_h:3700, Grid : 220 × 82 × 32, Smagorinsky model constant (C_s): 0.0065–0.01	Prescribed from LES of fully developed channel flow	7.18 (6.0)	No significant effect of C_s, mean velocity profiles in LES and DES match but not with exp., u' overpredicted by 50%, increased resolution had no effect on results. Inaccuracies attributed to precursor LES.
Aider & Danet, 2006 [35]	ER:1.2, Re_h:5100, Structure function model, grid not specified	Random noise (RN) or turbulence from precursor simulation (PS) introduced at $x = -2.5$h	RN : 5.8 (6.1), PS : 5.29 (6.1)	Different inflow conditions lead to significantly different shear layer flapping frequencies, coherent structures at the corner breakdown faster with latter inflow conditions
Panjwani et al., 2009, 2010 [31,37]	ER:1.2, Re_h:5100, Grid : 148 × 72 × 20, Structure function, Smagorinsky and dynamic Smagorinsky models	Random noise introduced at $x = -2.5$h	7.0–7.4 (6.1)	Numerical accuracy and grid refinement more important than LES modeling, predictions follow universal behavior when axial coordinate is scaled with X_r
Spode et al., 2005 [36]	ER:1.5, Re_h:5100, Grid : 384 × 96 × 64, Smagorinsky model constant = 0.1	White noise imposed over mean flow at $x = -$h	6.7(6.1), No model: 7.4 (6.1)	Second order statistics almost as good as in DNS
Kanchi et al., 2010 [38]	ER:1.2, Re_h:5100, M = 0.2, Chebyshev spectral method, Compressible dynamic Smagorinsky, explicit filtering LES models	Stochastic turbulence inflow model of Gao and Mashayek	5.98 (6.1)	Overprediction of v', Reynolds stresses, Both LES model lead to similar results
Patil et al., 2011 [15]	ER:9/8, Re_h:40000, Grid : 300 × 240 × 96, Dynamic Smagorinsky LES model with wall layer model	Inflow using synthetic eddy method (SEM) at $x = -4$h, Length scales for SEM obtained from LES of channel	6.3 (6.2)	Other than the maximum dip in C_f, all features well captured
Kanchi et al., 2011 [48]	ER:1.25, Re_h:28000, Chebyshev spectral (CS) compressible and Legendre spectral (LS) element incompressible solvers, explicit filtering LES model	Stochastic turbulence inflow model of Gao and Mashayek at $x = -10$h	CS : 6.85(6.7) LS : 5.69(6.7)	Grid refinement increased X_r further in of case of CS while reduced time step did not improve predictions of incompressible solver.
Kanchi et al., 2013 [23]	ER:1.2, Re_h:5100, Legendre spectral element solver, implicit LES	Random noise (RN), stochastic model (SM) of Gao and Mashayek at $x = -10$h	SM : 6.34 (6.1), RN : 7.35 (6.1)	Transitional nature of the recirculating flow not captured with larger time steps
Kanchi et al., 2013 [23]	ER:1.25, Re_h:28000, Legendre spectral element solver, implicit LES	Random noise RN), stochastic model (SM) of Gao and Mashayek at $x = -10$h	SM : 5.89 (6.7), RN : 6.49 (6.7)	Results less sensitive to inflow conditions than in low Re_h case although power spectra are different till the step
Sarwar et al., 2013 [39]	ER:1.2, Re_h:5100, Grid : 900 × 60 × 60, Smagorinsky, dynamic Smagorinsky, Deardorff Vreman LES models	Steady inflow at $x = -48$h , 2 mm trip wire used to transition the flow at $x = -40$h	Not noted	Smagorinsky model stated to be the most accurate
Sidik et al., 2013 [40]	ER:1.2, Re_h:5100, Grid : 300 × 60 × 40, Lattice Boltzmann solver, Smagorinsky model	Steady inflow at $x = -10$h	6.25 (6.1)	Reynolds stress overprediction within recirculation zone and underprediction at reattachment point significantly high

along the Mach lines. This leads to overprediction of turbulence levels in the recirculation zone. This is likely true with all synthetic turbulence techniques. Avoiding this problem would require combining these techniques with characteristic boundary conditions which has not been attempted so far.

Appendix A. Digital filtering technique

Inflow boundary is assumed to be planar and on the y-z plane here. Random numbers $r_{j,k}$ with a unit normal distribution are generated at all points on the inflow plane. "j" and "k" indicates coordinate points along the two cross stream (y- and z-) directions. The following filtering operation is used to spatially correlate the random numbers in these two directions.

$$u''_{j,k} = \sum_{p=-N}^{N} \sum_{q=-M}^{M} G_{j,k}(p) H_{j,k}(q) r_{j+p,k+q} \tag{2}$$

G and H are the filter coefficients is the two directions of the inflow plane. While Klein and coworkers [27] assumed Gaussian functional form for the auto-correlation, Xie and Castro [28] argued

that an exponential function is more appropriate.

$$\langle u''_{j,k} u''_{j+p,k} \rangle \sim exp\left[\frac{-\pi\,|(y_{j,k} - y_{j+p,k})|}{2L_y}\right] \tag{3}$$

An approximation to the filter that results in this correlation can be determined using explicit analytical expressions. The coefficients of filtering operation along y-direction ($G(p)$) are computed using these expressions.

$$\tilde{G}_{j,k}(p) = exp\left[\frac{-\pi(y_{j,k} - y_{j+p,k})}{L_y}\right] \tag{4}$$

$$G_{j,k}(p) = \tilde{G}_{j,k}(p)\left[\sum_{p=-N}^{N} [\tilde{G}_{j,k}(p)]^2\right]^{-1} \tag{5}$$

L_y is the integral length scale along the y-direction. Similarly, the coefficients for filtering along z-redirection can be computed for a given integral length scale L_z and filter function H.

The incoming flow also needs to temporally correlated so that the simulated flow inside the domain becomes spatially correlated along the axial direction.

$$u''' = u''_{old} exp\left(\frac{\pi\,\Delta t}{2\tau}\right) + u''\sqrt{1 - exp\left(\frac{\pi\,\Delta t}{\tau}\right)} \tag{6}$$

τ is the ratio of axial, integral length scale and the local mean convective velocity. For each velocity component, the three integral length scales have to be specified. For a general case, this may be a little difficult but for boundary layer type flows, the recommendations of Touber and Sandham [12] can be used for initial approximations.

The instantaneous velocity field is the sum of mean and fluctuation terms and is calculated as follows.

$$\begin{bmatrix} u \\ v \\ w \end{bmatrix} = \begin{bmatrix} U \\ V \\ V \end{bmatrix} + \begin{bmatrix} \sqrt{R_{11}} & 0 & 0 \\ R_{21}/\sqrt{R_{11}} & \sqrt{R_{22} - (R_{21}/\sqrt{R_{11}})^2} & 0 \\ 0 & 0 & \sqrt{R_{33}} \end{bmatrix} \times \begin{bmatrix} u''' \\ v''' \\ w''' \end{bmatrix} \tag{7}$$

u''', v''', w''' are all zero-mean, unit-variance random variables but not velocity fluctuations. Premultiplication of the vector with these variables with the matrix in the above equation results in the velocity fluctuation vector. This operation ensures that second moments of the velocity fluctuations are matched to corresponding prescribed elements of the Reynolds stress tensor. The above matrix is valid only in case with only one non-zero off-diagonal component of the Reynolds stress tensor. Xie and Castro [28] provided the matrix for the general case.

Touber and Sandham [12] used the strong Reynolds analogy (SRA) to generate thermodynamic fluctuations. As they pointed out, though SRA has been shown to be invalid for relating instantaneous quantities, it does provide a good estimate of variance of temperature fluctuations [12]. As a consequence, there may be additional delay in realizing truly turbulent flow due to the need for thermodynamics to adjust to the local flow field. Boundary layer approximation of constant pressure along wall-normal is used to specify the local density fluctuation.

$$\frac{T'}{\overline{T}} = (1 - \gamma)M^2 \frac{u'}{\overline{U}} \tag{8}$$

$$\frac{\rho'}{\overline{\rho}} = -\frac{T'}{\overline{T}} \tag{9}$$

As suggested by Touber and Sandham, the Box–Muller theorem is used for generating the random variables. Even with use of random numbers and two-dimensional filtering, they report that the computational cost of the digital filtering approach is not any higher than that of the synthetic turbulence approach based on analytical mode specification.

Appendix B. Literature survey of LES of subsonic flows over backward facing steps

See Table 2.

References

[1] T. Lund, X. Wu, D. Squires, Generation of turbulent inflow data for spatially-developing boundary layer simulations, J. Comput. Phys. 140 (1998) 233–258.
[2] P. Spalart, Direction numerical simulation of turbulent boundary layer up to $Re_\theta = 1410$, J. Fluid Mech. 187 (1988) 61–98.
[3] G. Urbin, D. Knight, Compressible large eddy simulation using unstructured grid : Boundary supersonic turbulent layer and compression corner, in: AIAA Paper 99-0427, 1999.
[4] H. Yan, D. Knight, A.A. Zheltovodov, Large-eddy simulation of supersonic flat-plate boundary layers using the monotonically integrated large-eddy simulation (MILES) Technique, Trans. ASME 124 (2002) 868–875.
[5] M.S. Loginov, N.A. Adams, A.A. Zheltovodov, Large-eddy simulation of shock-wave/turbulent-boundary-layer interaction, J. Fluid Mech. 565 (2006) 135–169.
[6] A. Hadjadj, Large eddy simulation of shock/boundary-layer interaction, AIAA J. 50 (2012) 2919–2927.
[7] P. Sagaut, E. Garnier, E. Tromeur, L. Larcheveque, E. Labourasse, Turbulent inflow conditions for large-eddy simulation of compressible wall-bounded flows, AIAA J. 42 (2004) 469–477.
[8] S. Xu, M.P. Martin, Assessment of inflow boundary conditions for compressible turbulent boundary layers, Phys. Fluids 16 (9) (2004) 3511–3523.
[9] W.A. El-Askary, Simulation of supersonic turbulent flow in the vicinity of an inclined backward-facing step, Int. J. Comput. Fluid Dyn. 25 (7) (2011) 407–423.
[10] A. Ferrante, S.E. Elghobashi, A robust method for generating inflow conditions for direct simulations of spatially-developing turbulent boundary layers, J. Comput. Phys. 198 (2004) 372–385.
[11] M. Pamies, P. Weiss, E. Garnier, S. Deck, P. Sagaut, Generation of synthetic turbulent inflow data for large eddy simulation of spatially evolving wall-bounded flows, Phys. Fluids 21 (2009) 379–385.
[12] E. Touber, N.D. Sandham, Large-eddy simulation of low frequency unsteadiness in a turbulent shock-induced separation bubble, Theor. Comput. Fluid Dyn. 23 (2009) 79–107.
[13] M. Grilli, P.J. Schmid, S. Hickel, N.A. Adams, Analysis of unsteady behavior in shockwave turbulent boundary layer interaction, in: Seventh European Symposium on Aerothermodynamics, Brugge, Belgium, 2011.
[14] N. Jarrin, S. Benhamadouche, D. Laurence, R. Prosser, A synthetic-eddy method for generating inflow conditions for large-eddy simulations, Int. J. Heat Fluid Flow 27 (2007) 585–593.
[15] S. Patil, D. Tafti, Wall modeled large eddy simulation of flow over a backward facing step with synthetic inlet turbulence, in: AIAA 2011-0747, 2011.
[16] Q. Zhang, W. Schröder, M. Meinke, A zonal RANS/LES method to determine the flow over a high-lift configuration, Comput. & Fluids 39 (2010) 1241–1253.
[17] B. Roidl, M. Meinke, W. Schröder, A zonal RANS-LES method for compressible flows, Comput. & Fluids 67 (2012) 1–15.
[18] B. Roidl, M. Meinke, W. Schröder, A reformulated synthetic turbulence generation method for a zonal RANS-LES method and its application to zero-pressure gradient boundary layers, Int. J. Heat Fluid Flow 44 (2013) 28–40.
[19] B. Roidl, M. Meinke, W. Schröder, Boundary layers affected by different pressure gradients investigated computationally by a zonal RANS-LES method, Int. J. Heat Fluid Flow 45 (2014) 1–13.
[20] A. Spille-Kohoff, H.-J. Kaltenbach, Generation of turbulent inflow data with a prescribed shear-stress profile, in: Second AFOSR International Conference on DNS/LES, Arlington, TX, USA, 2003.
[21] Z. Gao, F. Mashayek, Stochastic model for nonisothermal droplet laden turbulent flows, AIAA J. 42 (2004) 255–260.
[22] J. Volavy, M. Forman, M. Jicha, Turbulence forcing scheme in physical space based on ornstein-uhlenbeck process, in: ECCOMAS CFD, Lisbon, Portugal, 2010.
[23] H. Kanchi, K. Sengupta, F. Mashayrk, Effect of turbulent inflow boundary condition in LES of flow over a backward-facing step using spectral element method, Int. J. Heat Mass Transfer 62 (2013) 782–793.
[24] P. Batten, U. Goldberg, S. Chakravarthy, Interfacing statistical turbulence closures with large eddy simulation, AIAA J. 42 (2004) 485–492.
[25] A. Keating, U. Piomelli, Synthetic generation of inflow velocities for large-eddy simulation, in: AIAA Paper 2004-2547, 2004.

[26] N.D. Sandham, Y.F. Yao, A.A. Lawal, A large eddy simulation of transonic turbulent flow over a bump, Int. J. Heat Fluid Flow 24 (2003) 584–595.
[27] M. Klein, A. Sadiki, J. Janicka, A digital filter based generation of inflow date for spatially developing direct numerical or large eddy simulations, J. Comput. Phys. 186 (2003) 652–665.
[28] Z.T. Xie, I.P. Castro, Efficient generation of inflow conditions for large-eddy simulation of street-scale flows, Flow Turbulence Combust. 81 (2008) 449–470.
[29] V.K. Chakravarthy, K. Arora, D. Chakraborty, A simple hybrid finite volume solver for compressible turbulence, Internat. J. Numer. Methods Fluids 77 (12) (2015) 707–731.
[30] J. Smagorinsky, General circulation experiments with the primitive equations, Mon. Weather Rev. 91 (1963) 99–110.
[31] B. Panjwani, I.S. Ertesvag, A. Gruber, K.E. Rian, Large eddy simulation of backward facing step flow, in: 5th National Conference on Computational Mechanics, MekIT09, Trondheim, Norway, 2009.
[32] S. Jovic, D.M. Driver, Backward-facing step measurement at low Reynolds number, $Re_h = 5000$, in: Tech. Rep. NASA Technical Memorandum 108807, NASA, 1994.
[33] H. Le, P. Moin, J. Kim, Direct numerical simulation of turbulent flow over a backward-facing step, J. Fluid Mech. 330 (1997) 349–374.
[34] C. Benocci, R. Giammanco, M. Mamma, E. Simons, Large eddy simulation of turbulent ows via domain decomposition techniques. Part 2: Applications, Internat. J. Numer. Methods Fluids 48 (2005) 1–26.
[35] J.L. Aider, A. Danet, Large-eddy simulation study of upstream boundary conditions influence upon a backward-facing step flow, Comptes Rendus Mecanique 334 (2006) 447–453.
[36] C. Spode, R. Campregher, A.D. Neto, Parallel simulation of turbulent flow in a backward facing step, in: 18th International Congress of Mechanical Engineering, Ouro Preto, MG, 2005.
[37] B. Panjwani, I.S. Ertesvag, A. Gruber, K.E. Rian, Large eddy simulation in generalized curvilinear coordinates and its application to an axisymmetric dump combustor, in: ECCOMAS CFD, Lisbon, Portugal, 2010.
[38] H. Kanchi, K. Sengupta, G.B. Jacobs, F. Mashayek, Large-eddy simulation of compressible flow over backward-facing step using chebyshev multidomain method, in: AIAA Paper 2010-9222, 2010.
[39] M.M. Sarwar, K.A.M. Moinuddin, G.R. Thorpe, Large eddy simulation of flow over a backward facing step using fire dynamics simulator (FDS), in: 4th Asia Congress of Fluid Mechanics, Hanoi, Vietnam, 2013.
[40] N.A.C. Sidik, J. Ghaderian, S. Sadeghipour, Simulation of turbulent flow over a backward facing step using Lattice Boltzmann method, J. Eng. Sci. Technol. 8 (2013) 670–682.
[41] D.M. Kuehn, Effects of adverse pressure gradient on the incompressible reattaching flow over a rearward-facing step, AIAA J. 18 (3) (1980) 343–356.
[42] R. Marrano, R. Camarero, D. Pelletier, Large eddy simulation of turbulent flow over a backward facing step using the dynamic mixed model, in: AIAA 2001-2841, 2001.
[43] R.V.R. Avancha, R.H. Pletcher, Large eddy simulation of the turbulent flow past a backward facing step, in: AIAA 2010-0542, 2010.
[44] R.V.R. Avancha, R.H. Pletcher, Large eddy simulation of the turbulent flow past a backward-facing step with heat transfer and property variations, Int. J. Heat Fluid Flow 23 (2002) 601–614.
[45] Y. Dubief, F. Delcayre, On coherent-vortex identification in turbulence, J. Turbul. 1 (2000) 1–22.
[46] S. Saric, S. Jakirlic, C. Tropea, A periodically perturbed backward-facing step flow by means of LES, DES and T-RANS: An example of flow separation control, J. Fluids Eng. 127 (2005) 879–887.
[47] R.V. Westphal, J.P. Johnston, Effect of initial conditions on turbulent reattachment downstream of a backward facing step, AIAA J. 22 (1984) 1727–1732.
[48] H. Kanchi, F. Mashayek, K. Sengupta, G.B. Jacobs, P.F. Fischer, Comparison of LES studies in backward-facing step using Chebyshev multidomain and Legendre spectral element methods, in: AIAA Paper 2011-3557, 2011.
[49] A. Dejoan, Y.J. Yang, M.A. Leschziner, Comparative LES and unsteady RANS computations for a periodically-perturbed separated flow over a backward-facing step, J. Fluids Eng. 127 (2005) 872–878.
[50] I. Veloudis, Z. Yang, J.J. McGuirk, G.J. Page, A. Spencer, Novel implementation and assessment of a digital filter based approach for the generation of LES inlet conditions, Flow Turbulence Combust. 79 (2007) 1–24.
[51] R.L. Simpson, A model for the backflow mean velocity profile, AIAA J. 21 (1983) 142–143.
[52] K. Ishiko, T. Shimada, Implicit LES of compressible turbulent flow over a backward-facing step in the nozzle of solid rocket motor, in: AIAA Paper 2010-923, 2010.
[53] H. Liu, B. Wang, Y. Guo, H. Zhang, W. Lin, Effects of inflow mach number and step height on supersonic flows over a backward-facing step, Adv. Mech. Eng. 2013 (2013) 1–12.
[54] H. Ayyalasomayajula, S. Arunjatesan, C. Kannepalli, N. Sinha, Large eddy simulation of a supersonic flow over a backward-facing step for aero-optical analysis, in: AIAA Paper 2006-1416, 2006.
[55] D. Knight, H. Yan, A. Zheltovodov, Large eddy simulation of supersonic turbulent flow in expansioncompression corner, in: Third AFOSR International Conference on DNS/LES, Columbus, OH, USA, 2003.
[56] J. Fang, Y. Yao, A. Zheltovodov, Z. Li, L. Lu, Direct numerical simulation of supersonic turbulent flows around a tandem expansion-compression corner, Phys. Fluids 27 (2015) (published online).